Characterizing Snowpack with 60 GHz FMCW Millimeter-Wave Radar Sensors

Stijn Wielandt*, Ivo Marković*, Lonnie Chien*, Diana Morales*, Ryan Landon Crumley†, Baptiste Dafflon*, and Reynold Cooper‡
* *Earth and Environmental Sciences Area*, ‡ *Nuclear Sciences Division*
Lawrence Berkeley National Laboratory
Berkeley, CA, USA
† *Climate, Ecosystems, and Environmental Science*
Los Alamos National Laboratory
Los Alamos, NM, USA
Email: stijnwielandt@lbl.gov

***Abstract*—Snowpack is a vital component of Earth's hydrological cycle and one of the most sensitive to global warming. In order to develop a predictive understanding of the hydrological and biogeochemical dynamics in snow-dominated watersheds, scientists and water resources managers need spatially and temporally dense data sets of snowpack parameters, which could be obtained by networks of low-cost, low-power, distributed sensors. We investigate how 60 GHz frequency modulated continuous wave (FMCW) radar systems-on-chips (SoCs) can be used for measuring a variety of snowpack parameters. For snow depth measurements, we present a dedicated radar detection algorithm that detects the top of the observed snowpack, and we compare its performance to the established cell averaging constant false alarm rate (CA-CFAR) technique. We also evaluate the impact of non-coherent integration of radar frames over receive channels and over time. For measuring snow density and snow water equivalent (SWE), we rely on an adjustment for the signal's propagation speed in the snowpack based on prior knowledge about the radar's true distance to the ground. Our lab and field experiments show that snow layers can be detected, bulk snow density can be calculated, and the 90$^{\text{th}}$ percentile of snow depth measurement errors is 25 mm.**

***Index Terms*—FMCW Radar, Millimeter-Wave, Environment, Sensors, Snow, CFAR**

I. Introduction

More than one billion people on Earth rely on snowpack associated water supplies [1]. Snowmelt results in a steady and often yearlong water supply for streamflows and groundwater recharge. However, snowpack is one of the hydrological features most sensitive to global warming, resulting in growing impacts on communities, agriculture, infrastructure, and water resources management. An important focus of environmental research is improving the predictive understanding of the hydrological and biogeochemical dynamics in snow-dominated watersheds under a changing climate, which requires spatially and temporally dense measurements of snowpack characteristics [2]. Snow depth ($\bar{d}$) is an important parameter that indicates the thickness of the snowpack, measured from the ground up. Snow water equivalent (SWE) is expressed in mm and represents the depth of a hypothetical water column after melting the snowpack. The density of snow (ρ) is defined as the snow mass (m_s) in a control volume (V), with common values in the 80–600 kg/m^3 range. The snow density averaged over the depth ($\bar{\rho}$) is referred to as the bulk density and is related to SWE and $\bar{d}$ as expressed in (1).

$$\text{SWE} = \bar{\rho}\bar{d} \tag{1}$$

Other parameters of interest include thermal characteristics and snow stratigraphy, i.e. the structure of snowpack with layers of varying height, density, hardness, grain size, and crystal shape [3]. Snow stratigraphic observations still rely on manual methods that include digging snow pits and an often visual or manual assessment of layer parameters, as described in the International Classification for Seasonal Snow on the Ground [4]. Because of this manual and invasive approach, measurements are spatially and temporally sparse, and not repeatable. Satellite and airborne observations provide an alternative, non-invasive solution to increase the spatial coverage of snow observations. However, these observations are often characterized by high uncertainties for SWE measurements, coarse spatial resolutions (tens of km), low temporal resolutions, and impacts of cloud cover [5]. In-situ sensors can provide an outcome for highly accurate observations with a high temporal resolution. Snow pillows and scales are standard instruments for accurate SWE measurements, but their cost and installation efforts prevent spatially dense observations. Snow depth is commonly measured using ultrasonic ranging sensors, but the technology requires a correction of the acoustic propagation speed based on atmospheric temperature and humidity, and the accuracy of the results is also affected by wind, snowfall, and the density of the top layer of the snowpack [6]. Optical systems (e.g., laser based) form an alternative, but these are also sensitive to atmospheric processes and come at a high cost

This work was supported by the Laboratory Directed Research and Development Program of Lawrence Berkeley National Laboratory, and the U.S. Department of Energy, Office of Science, Office of Biological and Environmental Research, Next-Generation Ecosystem Experiments–Arctic Project (NGEE-Arctic) under U.S. Department of Energy Contract No. DE-AC02-05CH11231.

and power consumption [7]. In recent research, novel, low-cost methods have been investigated to facilitate spatiotemporally dense observations using wireless sensor networks. Dafflon et al. [8] presented a low-cost probe for thermal snowpack analysis and snow height estimation, but the accuracy of the system depends on sensor spacing and the impact of the instrument on the snowpack is still to be investigated. Other relevant techniques rely on the radio frequency (RF) propagation characteristics of snowpack to gain insights into SWE and layer structures. Le Breton et al. presented an RFID based system that measures RF signal phase differences introduced by the snowpack for RFID tags at different depths [9]. Based on these measurements, the snowpack permittivity can be determined, which is a function of ρ. Steiner et al. also rely on snowpack permittivity to calculate SWE based on the signal delays measured by buried GPS stations [10]. In the same context, radar technology has garnered considerable interest for observing snowpack over the past few decades. Pulsed (ground penetrating) radar technology has been used for snow stratigraphy [11] and tomographic imaging [12]. However, the pulsed operation and sub-GHz frequency range of these systems results in a limited resolution of the observations, a large instrument footprint, and a high power consumption and cost [13]. In a frequency modulated continuous wave (FMCW) radar system a chirp is transmitted by the radar, reflected by the environment, and received again by the radar. By down mixing the transmitted and received waveforms, an intermediate frequency (IF) signal is created that can easily be sampled. The IF signal's frequency components (f_{IF}) are directly proportional to the reflectors' distances and the chirp bandwidth (β) determines the range resolution. Previous research on the use of FMCW radars for snow stratigraphy has used L-band radars [14], but Koh et al. demonstrated that higher frequencies (up to Ka band) can provide more detailed insights in snowpack structure [15]. The widespread adoption of FMCW radars for spatiotemporally dense snowpack observations has been hindered by the cost, footprint, and complexity of these systems. However, recent developments in the field of millimeter-wave (mmWave) sensing have resulted in the commercial availability of low-cost, highly integrated FMCW radar systems-on-chips (SoCs) [16]. These chips usually operate in the 60 GHz ISM band (or the 77 GHz automotive radar band), support bandwidths exceeding 4 GHz, and house the entire analog, digital, and signal processing chain, which can even include antenna arrays (i.e. antenna in package (AiP)). A radar system based on these FMCW SoCs is characterized by a low cost, limited power consumption, small size, low complexity, and compatibility with the 60 GHz ISM band, which opens opportunities for wireless sensor networks for spatiotemporally dense observations of snowpack characteristics. In this paper, we present how a 60 GHz FMCW radar SoC can be used for measuring snow depth, SWE, and snowpack stratigraphy, based on lab and field experiments.

II. Proposed method

For our research we employ an Infineon XENSIV™ BGT60TR13C [17] FMCW radar SoC on an Infineon DEMO BGT60TR13C board. This chip was selected because it provides a bandwidth of 5.5 GHz in the 60 GHz band, and it houses all functionality on-chip, including one transmit antenna and three receive antennas with 12-bit ADCs. Furthermore, the availability of low-cost, low-power development platforms and data acquisition software accelerates the development of environmental sensor devices. An important drawback of this system in comparison to other radar SoCs is that it only samples in-phase signal components, reducing phase coherent processing capabilities like beam forming. In our experiments, the board was covered with a 0.254 mm thick LDPE film for waterproofing with minimal RF impact [18]. All experiments in this paper were performed at temperatures $< 0°$C to ensure the absence of liquid water. In order to maximize the accuracy of our measurements in the context of the snowpack parameters under investigation ($\bar{d}$, $\bar{\rho}$, SWE, layer structure) we aim for a maximal range resolution (ΔR) and minimal range bin size (ΔR_{s}), which is achieved by using the maximal frequency range of the chip (58.0 GHz – 63.5 GHz), while maximizing the sample frequency ($f_{\mathrm{s}} = 2.5$ Msps) and chirp duration (512 samples). In vacuum and by approximation in air the (real) relative permittivity is $\varepsilon_{\mathrm{r}} = 1$, which results in a range resolution of 0.0272 m, a range bin size of 0.0136 m, and a maximum range detection of 6.98 m [19]. In order to maximize the signal-to-interference ratio (SIR), we maximize the transmit power ($P_{\mathrm{Tx}} = 31$ dBm) and we activate all three receive channels, which allows for signal integration over space. In our experiments, each acquired radar frame contains 256 chirps, which affects doppler velocity capabilities. However, doppler velocity measurements are considered irrelevant to this research since all measurement scenarios are static.

A. Snow Depth Sensing

In order to evaluate the snow depth measurement capabilities of the considered radar hardware, we built a measurement setup in Nome, AK as presented in Fig. 1(A). The setup consists of a pile of snow with a flat top (2 m diameter) and $\bar{d} \approx 0.95$ m. A downward looking radar was mounted at seven discrete heights above the snow pile ($x_{\mathrm{snow}} = \{0.24, 0.39, 0.53, 0.63, 0.73, 1.31, 1.64\}$ m) and experiments were performed in snowy, windy weather, with a top snow pile layer of both fresh undisturbed snow, and compacted snow. For each height, 4 data sets of 100 frames were acquired separately, resulting in a total data set of 2,800 radar frames. $\bar{d}$ can easily be calculated as the difference between the height of the radar (which is supposed to be known) and the measured range to the top of the snowpack ($\hat{x}_{\mathrm{snow}}$). Fig. 2 illustrates a radar range profile ($R(x)$, where x represents the distance from the radar) for a single receive channel with the radar mounted 0.53 m above the snow pack. The curve shows an initial DC peak, followed by a dip that demonstrates the lack of reflections in air. The air-snowpack interface is characterized by a strong reflection, followed by

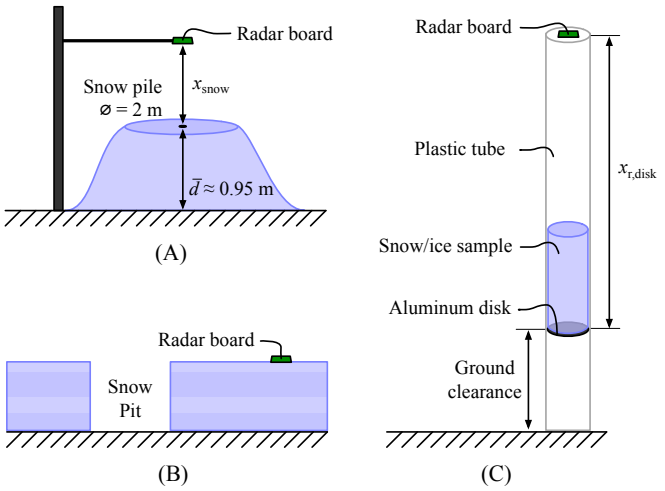

Fig. 1. Measurement setups for (A) snow depth measurement of a snow pile in Nome, AK, (B) SWE and snowpack stratigraphy near Nome, AK, (C) SWE and snowpack stratigraphy in a lab setting.

multiple reflections originating from within the snowpack and subsurface. In order to accurately measure the distance to the air-snowpack interface, we need a peak detection algorithm that accurately identifies the associated reflection in the curve.

Constant false-alarm rate (CFAR) detection is a common approach for radar peak finding because it takes variable interference levels into account [20]. The established cell-averaging CFAR (CA-CFAR) detector is used as a benchmark in this research. For each range bin value (the cell under test), the interference power is estimated ($\bar{P}_{\text{i}}$) by averaging a certain number (N) of neighboring reference cells. This excludes N_{guard} guard cells on each side of the cell under test because a target reflection could span multiple range bins. A detection threshold T is determined as a function of a false alarm probability (P_{FA}) as defined in (2):

$$T = \bar{P}_{\text{i}} \cdot N \cdot \left(P_{\text{FA}}^{-1/N} - 1 \right) \tag{2}$$

CA-CFAR is supposed to detect any radar target, which means the algorithm can return multiple peaks or no peak at all ($x_{\text{CFAR}} = \{\dots\}$), as demonstrated in Fig. 2. In our application, we are only interested in the air-snow boundary (x_{snow}), so we decided to estimate it as either the first ($\hat{x}_{\text{snow,first}} = x_{\text{CFAR}}[1]$) or the highest CA-CFAR peak ($\hat{x}_{\text{snow,max}} = \text{argmax}(R(x_{\text{CFAR}}))$. When no peak is detected, we assume $\hat{x}_{\text{snow}} = 0$.

As for the CA-CFAR parameters, we arbitrarily selected $N = 10$ to ensure sufficient impact of the deep dip in the range curve while reducing the impact of the DC peak, and $N_{\text{guard}} = 4$ to take into account snow surface roughness while avoiding reflections from within the snowpack. We evaluate the algorithm for $P_{\text{FA}} = 0.1\%$ and $P_{\text{FA}} = 1\%$ to evaluate the trade-off between false positives and undetected peaks.

Since the number of returned peaks from the CA-CFAR algorithm is unpredictable and we are only interested in one strong reflection from the air-snow interface, we propose a different method. First, we determine the range value with the steepest upslope (x_{up}) in the range plot (3). Then we find the next local maximum, which is our estimated range to the snowpack ($\hat{x}_{\text{snow,up}}$) (4).

$$x_{\text{up}} = \text{argmax}_x(\nabla R) \tag{3}$$

$$\hat{x}_{\text{snow,up}} = \min_{\forall\, x > x_{\text{up}}} \{x \mid \nabla R = 0\} \tag{4}$$

In order to reduce the impact of interference and improve the accuracy of snow depth detection, we investigate the impact of averaging signals over multiple receive channels and over time. Since the used platform does not perform coherent IQ sampling, we only study non-coherent signal integration [20].

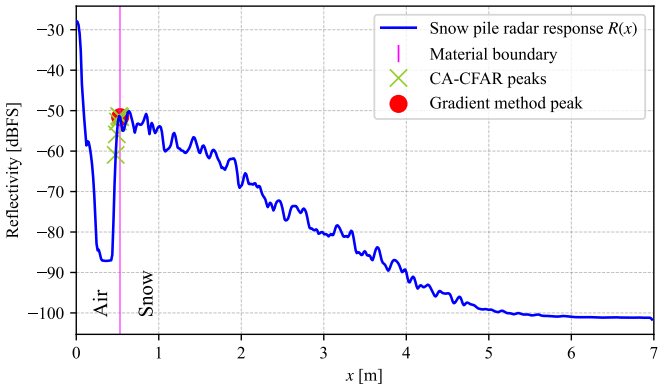

Fig. 2. Example range plot for the Infineon BGT60TR13C positioned 0.53 m above a snow pile.

B. Snow Density

The IF signal's frequency f_{IF} that is sampled by the FMCW radar as a result of a reflection from a target at a distance x_{r} is described by (5) [15], where c represents the speed of light in vacuum, and T_{s} is the chirp sweep time. In most radar applications, the signal travels through air and the only unknown parameter is the range x_{r}, which is directly proportional to f_{IF}.

$$f_{\text{IF}} = \frac{2\beta x_r \sqrt{\varepsilon_{\text{r}}}}{\text{c} T_{\text{s}}} \tag{5}$$

When the signal travels through snowpack, ε_{r} becomes an unknown. According to Tiuri et al., ε_{r} for dry snow (i.e., not containing liquid water) can be modeled by a second order polynomial (6) [21]. The authors verified this relationship for frequencies of 850 MHz up to 12.6 GHz, and it was also determined that ε_{r} depends almost solely on the density ρ; no impact was observed for differences in snow crystal structure or grain size, age, and hardness.

$$\varepsilon_{\text{r,snow}} = 1 + 1.7\rho + 0.7\rho^2 \tag{6}$$

Following (5) and (6), our FMCW radar system can be used to measure ρ when x_{r} is a known parameter. In practice, this means that a standard radar range measurement (assuming

$\varepsilon_{\mathrm{r}} = 1$) can be corrected to find the actual $\varepsilon_{\mathrm{r,snow}}$, which in turn leads to $\bar{\rho}$. With both range and density information being known, we can calculate SWE using (1). However, we need to evaluate if (6) also holds for measurements in the 60 GHz band. In order to test this, we perform experiments with various known snow densities and known x_{r}. Fig. 1(C) presents our lab setup, consisting of a radar aimed into a PVC tube ($\varepsilon_{\mathrm{r,PVC,60\ GHz}} \approx 4$ [18], 40 mm inner diameter, 4 mm wall thickness, 1.585 m length), an aluminum disk at $x_{\mathrm{r,disk}} = 0.785$ m, and a sample core (225 mm length) placed on the aluminum disk. The use of a plastic tube (over a metallic waveguide for example) ensures that multipath reflections off the tube's walls are weak, and the ground clearance of the aluminum disk eliminates interference from ground reflections. Since ε_{r} depends almost solely on ρ, we can perform our experiments with cores of artificial snow. We evaluate a low-density snow core ($\rho_1 = 130\ \mathrm{kg/m^3}$), a high-density snow core ($\rho_2 = 520\ \mathrm{kg/m^3}$), and an ice core ($\rho_3 = 910\ \mathrm{kg/m^3}$).

C. Snowpack Stratigraphy

While ε_{r} is only a function of ρ, other snow parameters (e.g., crystal size) do affect signal reflectivity and attenuation. This means that each layer within the snowpack will have different signal absorption and reflection characteristics that affect the radar response, so we aim to capture this phenomenon in the 60 GHz band. First, we evaluate the radar response of the homogeneous snow and ice cores in the lab, as discussed in Section II-B. Next, we test an artificial core consisting of multiple homogeneous layers: a top snow layer of 150 mm ($\rho_{\mathrm{top}} = 115\ \mathrm{kg/m^3}$), followed by a 50 mm ice layer ($\rho_{\mathrm{mid}} = 910\ \mathrm{kg/m^3}$), and a bottom snow layer of 100 mm ($\rho_{\mathrm{bottom}} = 520\ \mathrm{kg/m^3}$). For practical reasons, this test was performed using a transparent acrylic tube ($\varepsilon_{\mathrm{r,acrylic,60\ GHz}} \approx 2.6$ [18], 50 mm inner diameter, 5 mm wall thickness, 1.390 m length), with the aluminum disk at $x_{\mathrm{r,disk}} = 0.955$ m. Finally, we evaluate the radar's performance for snow stratigraphy in the field. We conducted a snow pit study in Nome, AK, gathering information on snow layer thickness, density, hardness, and temperature. As illustrated in Fig. 2(B), we performed a radar measurement at the same site; for practical reasons we placed the radar face-down on the snowpack, 1.5 m away from the snow pit. All snowpack stratigraphy experiments involve a correction for the snow density, so these tests also double as an extra evaluation of our snow density measurement capabilities.

III. Experimental Data and Results

A. Snow Depth Sensing

Table I lists the statistics of snow depth measurement errors (absolute values) for the CA-CFAR and gradient based detection algorithms, based on the measurements of 2,800 radar frames at the presented seven heights above the snowpack. In order to reduce interference, all results presented in this table were based on radar profiles averaged over all three receive channels. The impact of this averaging operation is presented separately in Table II and discussed in the next paragraph. All median error values across the considered algorithms are below 0.05 m, which demonstrates the general capability of the algorithms for snowpack ranging. Based on the 50$^{\text{th}}$ percentiles, one could also conclude that a CA-CFAR based algorithm provides better results for $\hat{x}_{\mathrm{snow,max}}$ than $\hat{x}_{\mathrm{snow,first}}$. However, CA-CFAR based methods demonstrate very high error levels in the 90$^{\text{th}}$ and 95$^{\text{th}}$ percentiles. For the $P_{\mathrm{PA}} = 0.1\%$ configuration these percentiles line up with the 0.24 m and 1.60 m measurement heights, indicating that the CA-CFAR algorithm did not detect any radar targets and $\hat{x}_{\mathrm{snow}} = 0$ for these setups. Reducing the CA-CFAR threshold ($P_{\mathrm{PA}} = 1\%$) results in the actual detection of peaks, but these peaks often don't line up with the top of the snowpack, resulting in an overall low performance of the CA-CFAR algorithm for this application. The gradient based peak detection algorithm is tailored to our application and always produces a single result, which clearly yields superior performance to the CA-CFAR based methods. One can observe that the median error for $\hat{x}_{\mathrm{snow,up}}$ is smaller than ΔR_{s}, which can be explained by the close alignment of some of our 7 test setups with the range bins.

TABLE I
Accuracy of snow depth measurements for the proposed CA-CFAR and gradient based algorithms.

Algorithm:		$\hat{x}_{\mathrm{snow,max}}$		$\hat{x}_{\mathrm{snow,first}}$		$\hat{x}_{\mathrm{snow,up}}$
		$P_{\mathrm{PA}} = 1\%$	0.1%	$P_{\mathrm{PA}} = 1\%$	0.1%	
$\lvert\mathrm{Error}\rvert$ [m]	Mean	0.165	0.161	0.150	0.180	0.076
	Std.	0.383	0.426	0.335	0.418	0.314
	P50	0.011	0.011	0.047	0.038	0.002
	P90	0.397	0.240	0.240	0.240	0.053
	P95	1.091	1.600	1.063	1.600	0.454

The BGT60TR13C has three receive antennas, so we evaluate the performance of each channel separately, and we evaluate the impact of averaging range profiles over all three channels. Table II presents the ranging errors for these scenarios, indicating slightly better performance for radar channel 3, but overall there is a considerable number of large errors as demonstrated by the 90$^{\text{th}}$ and 95$^{\text{th}}$ percentiles. Averaging a radar frame's range profiles over all channels significantly reduces these larger errors and results in a 90$^{\text{th}}$ percentile snowpack ranging accuracy of 0.053 m.

TABLE II
$\hat{x}_{\mathrm{snow,up}}$ errors for different radar channels and their averaged radar response.

Channel:		1	2	3	Averaged
$\lvert\mathrm{Error}\rvert$ [m]	Mean	0.189	0.176	0.134	0.076
	Std.	0.415	0.442	0.434	0.314
	P50	0.006	0.007	0.001	0.002
	P90	0.943	0.698	0.238	0.053
	P95	1.241	1.412	1.241	0.454

All previously discussed results were obtained by considering radar frames separately. In Table III we evaluate the impact of non-coherent integration of multiple radar frames (i.e. averaging). While the acquisition of multiple radar frames results in an increased power consumption, our results show that

the snowpack ranging accuracy can significantly be improved. Especially the sporadic, large errors represented by the 95$^{\text{th}}$ percentile can be reduced tenfold by averaging, improving the accuracy in that percentile to 0.042 m. If power consumption is a concern, at least 2 radar frames should be averaged, since this results in the most dramatic improvement of the 95$^{\text{th}}$ error percentile.

TABLE III
$\hat{x}_{\text{snow,up}}$ ERRORS WITH NON-COHERENT INTEGRATION OF MULTIPLE RADAR FRAMES OVER TIME.

# frames:		1	2	4	8	16	32
|Error| [m]	Mean	0.076	0.049	0.027	0.027	0.024	0.019
	Std.	0.314	0.242	0.172	0.169	0.155	0.128
	P50	0.002	0.002	0.002	0.002	0.002	0.002
	P90	0.053	0.039	0.025	0.025	0.025	0.025
	P95	0.454	0.066	0.053	0.053	0.053	0.042

When comparing our results to literature, we find that the invasive snow probes reported in [8] provide a much lower measurement resolution of 5 to 10 cm. The laser based solution presented in [22] has mean error levels of 4.5 cm, which is higher than the 1.9 cm we achieve when integrating multiple radar frames. Most importantly, our results show that low-cost, low-power 60 GHz FMCW radar SoCs can be a solution for accurate, in-situ snow depth measurements with high spatiotemporal densities and reliable operation, even in windy and snowy weather conditions.

B. Snow Density

In order to assess the snow density sensing capabilities of the 60 GHz radar, we evaluate the results from the three lab experiments with homogeneous snow/ice cores. Fig. 3 depicts the uncorrected radar range profiles (assuming $\varepsilon_{\text{r}} = 1$) as dashed lines, while the solid curves represent a corrected range profile based on (6) and the known values of ρ_1, ρ_2, and ρ_3. All curves exhibit a clear peak at the air-snow/ice interface, and –in contrast to the uncorrected radar range profiles– the adjusted curves have their next peak aligned exactly with the location of the aluminum disk. The precise alignment of this correction demonstrates that we are effectively correcting for the slower propagation speed, and that (6) can be used in the 60 GHz band for a wide range of ρ values. This also means that the same technique can be inverted to measure SWE: Section III-A demonstrated that we can measure $\bar{d}$, and prior knowledge about the true distance to ground enables a range adjustment that yields $\bar{\rho}$, and consecutively SWE (1).

C. Snowpack Stratigraphy

The results in Fig. 3 demonstrate how a homogeneous snow/ice core yields a clear radar response at the material boundaries. Fig. 4 presents the results from an artificial core that consists of three homogeneous layers with varying density, hardness, and grain size. The results show how all material boundaries consistently align with the peaks in the corrected radar profile, confirming not only the validity of (6) for propagation speed adjustments, but also that material interfaces within the snowpack produce clear radar responses.

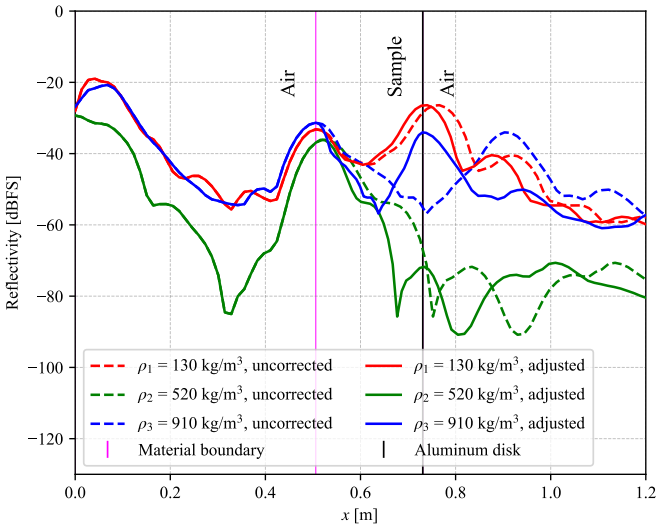

Fig. 3. Uncorrected radar range profiles (assuming $\varepsilon_{\text{r}} = 1$) for three snow/ice lab samples, and their adjusted versions that take ρ into account.

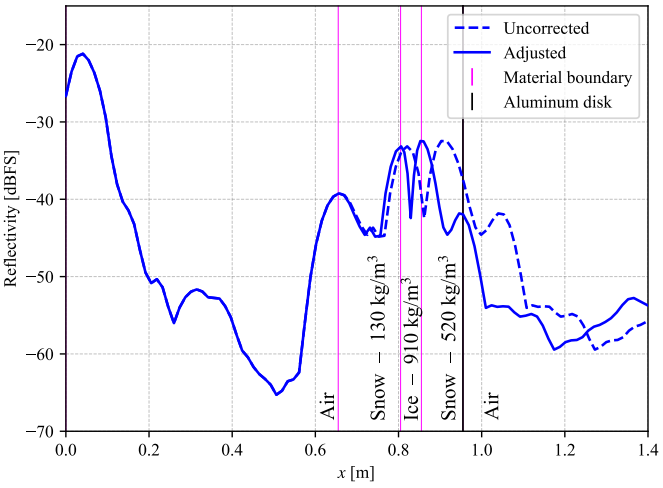

Fig. 4. Standard radar range profile for a three-layer artificial core, and its adjusted version that takes ρ_{top}, ρ_{mid}, and ρ_{bottom} into account.

Fig. 5 visualizes the results from manual examinations in a snow pit, and a co-located radar measurement. The snowpack temperature ranges from -6°C to -2°C, and while the hardness exhibits some variability (reported according to [4]), the density is more or less constant. The adjusted radar response has a significant peak coinciding with the ground interface, confirming that $\bar{\rho}$ can actually be measured in realistic environments with prior knowledge of the distance to ground. When observing material boundaries, some agreement can be found with a peak and an inflection point of the adjusted radar range profile, but the overall agreement between radar peaks and snow pit observations is limited, which could be explained as follows. First, there is the limited variability in snow characteristics (e.g., no ice layers were observed) and no metal target (cfr. aluminum disk) was present at the snow-ground interface, which explains why no particularly

strong features in the radar profile are observed. Second, a significant number of peaks can be observed within snow layers, which contrasts lab tests. This could be explained by the small sample size and coarse resolution of manual snow pit observations (5-10 cm), while the radar observes an entire snowpack volume with cm-resolution and high sensitivity to perturbations because of the short wavelength [2].

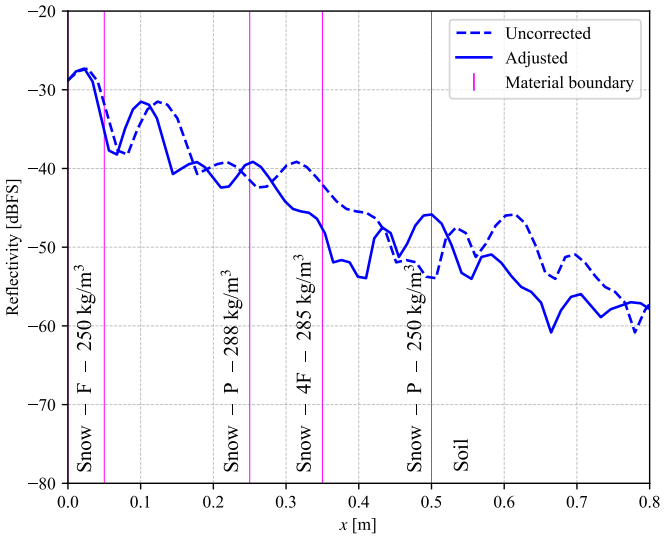

Fig. 5. Radar range profiles and co-located snow pit measurements.

IV. Conclusions and Future Work

Our evaluation of a snowpack sensor based on a 60 GHz FMCW radar SoC shows that these systems form a promising solution for large-scale deployments of low-cost, low-complexity, and low-power in-situ snowpack sensors for spatiotemporally dense measurements. Our experiments indicate a 90^{th} percentile snow depth measurement error of 25 mm when we use a dedicated peak detection algorithm that outperforms CA-CFAR, and when we average radar frames over time and over receive channels. Our lab and field experiments also demonstrate that $\bar{\rho}$ and SWE can be calculated by performing an adjustment for the signal's propagation speed with prior knowledge about the snow-ground interface, which is generally available in fixed deployments. While lab experiments clearly demonstrate that 60 GHz radars can be used for snow layer detection, further field experiments are needed to investigate how these systems can be used for in-situ snow stratigraphy. Future work will focus on long-term field experiments that include buried reflective targets. We will also assess the maximal propagation distance of a radar signal in snowpack, and assess the impact of wet snow.

References

[1] K. N. Musselman, N. Addor, J. A. Vano, and N. P. Molotch, "Winter melt trends portend widespread declines in snow water resources," *Nature Climate Change*, vol. 11, no. 5, pp. 418–424, 2021.

[2] N. J. Kinar and J. W. Pomeroy, "Measurement of the physical properties of the snowpack," *Reviews of Geophysics*, vol. 53, no. 2, pp. 481–544, 2015. [Online]. Available: https://agupubs.onlinelibrary.wiley.com/doi/abs/10.1002/2015RG000481

[3] P. W. Nienow and F. Campbell, *Stratigraphy of Snowpacks*. Dordrecht: Springer Netherlands, 2011, pp. 1081–1084. [Online]. Available: https://doi.org/10.1007/978-90-481-2642-2_541

[4] C. Fierz, R. L. Armstrong, Y. Durand, P. Etchevers, E. Greene, D. M. McClung, K. Nishimura, P. K. Satyawali, and S. A. Sokratov, "The international classification for seasonal snow on the ground," 2009.

[5] R. Pirazzini, L. Leppänen, G. Picard, J. I. Lopez-Moreno, C. Marty, G. Macelloni, A. Kontu, A. Von Lerber, C. M. Tanis, M. Schneebeli, P. De Rosnay, and A. N. Arslan, "European in-situ snow measurements: Practices and purposes," *Sensors*, vol. 18, no. 7, 2018. [Online]. Available: https://www.mdpi.com/1424-8220/18/7/2016

[6] H. Gubler, "An inexpensive remote snow-depth gauge based on ultrasonic wave reflection from the snow surface," *Journal of Glaciology*, vol. 27, no. 95, pp. 157–163, 1981.

[7] M. Adams, E. Gleirscher, T. Gigele, and R. Fromm, "Automated terrestrial laser scanner measurements of small-scale snow avalanches," in *Proc. Intern. Snow Science Workshop Grenoble–Chamonix MontBlanc*, 2013, pp. 1060–1065.

[8] B. Dafflon, S. Wielandt, J. Lamb, P. McClure, I. Shirley, S. Uhlemann, C. Wang, S. Fiolleau, C. Brunetti, F. H. Akins, J. Fitzpatrick, S. Pullman, R. Busey, C. Ulrich, J. Peterson, and S. S. Hubbard, "A distributed temperature profiling system for vertically and laterally dense acquisition of soil and snow temperature," *The Cryosphere*, vol. 16, no. 2, pp. 719–736, 2022. [Online]. Available: https://tc.copernicus.org/articles/16/719/2022/

[9] M. Le Breton, E. Larose, L. Baillet, Y. Lejeune, and A. van Herwijnen, "Monitoring snow water equivalent using the phase of rfid signals," *The Cryosphere*, vol. 17, no. 8, pp. 3137–3156, 2023. [Online]. Available: https://tc.copernicus.org/articles/17/3137/2023/

[10] L. Steiner, M. Meindl, C. Fierz, C. Marty, and A. Geiger, "Monitoring snow water equivalent using low-cost gps antennas buried underneath a snowpack," in *2019 13th European Conference on Antennas and Propagation (EuCAP)*, 2019, pp. 1–5.

[11] J. T. Harper and J. H. Bradford, "Snow stratigraphy over a uniform depositional surface: spatial variability and measurement tools," *Cold Regions Science and Technology*, vol. 37, no. 3, pp. 289–298, 2003, iSSW 2002: International Snow Science Workshop. [Online]. Available: https://www.sciencedirect.com/science/article/pii/S0165232X03000715

[12] R. Fortin and R. Fortier, "Tomographic imaging of a snowpack," in *Proceedings of the 58th Annual Eastern Snow Conference*, 2001, pp. 17–19.

[13] H. Meikle, *Modern radar systems; 2nd ed.* Norwood: Artech House, 2008. [Online]. Available: https://cds.cern.ch/record/1608391

[14] N. Yankielun, W. Rosenthal, and R. E. Davis, "Alpine snow depth measurements from aerial fmcw radar," *Cold Regions Science and Technology*, vol. 40, no. 1, pp. 123–134, 2004. [Online]. Available: https://www.sciencedirect.com/science/article/pii/S0165232X04000606

[15] G. Koh, N. E. Yankielun, and A. I. Baptista, "Snow cover characterization using multiabnd fmcw radars," *Hydrological Processes*, vol. 10, no. 12, pp. 1609–1617, 1996.

[16] A. Shastri, N. Valecha, E. Bashirov, H. Tataria, M. Lentmaier, F. Tufvesson, M. Rossi, and P. Casari, "A review of millimeter wave device-based localization and device-free sensing technologies and applications," *IEEE Communications Surveys Tutorials*, vol. 24, no. 3, pp. 1708–1749, 2022.

[17] Infineon Technologies AG, "BGT60TR13C 60 GHz Radar Sensor Datasheet V2.4.8 Full," 2023. [Online]. Available: https://www.infineon.com/cms/en/product/sensor/radar-sensors/radar-sensors-for-iot/60ghz-radar/bgt60tr13c

[18] A. J. Bur, "Dielectric properties of polymers at microwave frequencies: a review," *Polymer*, vol. 26, no. 7, pp. 963–977, 1985.

[19] M. Jankiraman, "Fmcw radar design, artech house," *Norwood, Ma*, 2018.

[20] M. A. Richards *et al.*, *Fundamentals of radar signal processing*. Mcgraw-hill New York, 2005, vol. 1.

[21] M. Tiuri, A. Sihvola, E. Nyfors, and M. Hallikaiken, "The complex dielectric constant of snow at microwave frequencies," *IEEE Journal of Oceanic Engineering*, vol. 9, no. 5, pp. 377–382, 1984.

[22] A. Prokop, M. Schirmer, M. Rub, M. Lehning, and M. Stocker, "A comparison of measurement methods: terrestrial laser scanning, tachymetry and snow probing for the determination of the spatial snow-depth distribution on slopes," *Annals of Glaciology*, vol. 49, p. 210–216, 2008.